

Automatic localization and delineation of collimation fields in digital and film-based radiographs

Thomas M. Lehmann^{*}, Sascha Goudarzi, Nick I. Linnenbrügger,
Daniel Keysers^a, Berthold B. Wein^b

Institute of Medical Informatics

^aChair of Computer Science VI

^bDepartment of Diagnostic Radiology

Aachen University of Technology (RWTH), Aachen, Germany

ABSTRACT

Collimation field detection is an important pre-processing step for automatic image analysis of radiographs. However, most approaches are restricted to a small set of form archetypes or presuppose the presence of a shutter. Hence, existing methods are not applicable to large collections of radiographs from various modalities, such as obtained in the field of content-based image retrieval in medical applications. Based on analytical evaluation, the approach of WIEMKER *et al.* (Procs SPIE 2000; 3979:1555–1565) was selected, modified in order to reduce false positive detection, and evaluated on a large set of 4,000 radiographs (763 containing shutter edges) taken from daily routine including any kind of projective X-ray examinations. Eight subsets (each of 500 images) were compiled randomly. A set of 500 images was used to optimize the parameters and evaluated using the remaining 3,500 images. This procedure was repeated for all eight combinations. Using the initial approach, the specificity is 96.4% with a poor sensitivity of 44.1% resulting in an overall precision of 86.7%. All figures increase up to 98.5%, 55.6%, and 89.5%, respectively, if the algorithm also minimizes the variation of radiation density values outside the detected shutter area. In terms of sensitivity and precision, the results of optimization vs. evaluation for the same combination and of evaluation vs. evaluation for different combinations differed up to 13 and 9 percentage points, respectively. This indicates that still an insufficient number of images is used to allow complete generalization of the results.

Keywords: Radiation Field Recognition, Collimation Detection, Shutter Removal, Background Removal, Hough-Transform, Content-Based Image Retrieval, Software Evaluation

1. INTRODUCTION

Within a medical image, which has either been digitally recorded or secondarily digitized, not all pixels host information of diagnostic relevance. For example, patients are protected against unnecessary exposure to X-rays by use of radiopaque material, which is placed in between the beam pathways from the X-ray to the patient. This process is referred to as collimating and the radiopaque material is named collimator or shutter,⁴ while the area under normal exposure is called the radiation field¹³ or irradiation field.⁴ Some modalities, e.g., fluoroscopy, have a non-rectangular aperture that covers parts of the screen. If film-based X-ray examinations are digitized, masking effects are also induced from the scanning process. In the following, we summarize all these different effects within the term "collimation field". Sometimes, a larger part of the film is shielded to be exposed separately in a second examination. This process is referred to as partitioning,⁴ but is disregarded in this investigation.

Collimation field detection in radiographs is an important pre-processing step for automatic image analysis, indexing and retrieval.¹¹ Global measures of gray scale, texture, or structure are altered when the collimation field covers a substantial part of the digital image. Several methods for automatic segmentation have been suggested.^{2,3,10,11,13-15}

^{*} lehmann@computer.org; phone +49 241 80-88793; fax +49 241 80-82426; <http://www.irma-project.org>; Institute of Medical Informatics, Aachen University of Technology, Pauwelsstr. 30, D - 52057 Aachen, Germany.

Usually, the process of segmentation is comprised of two steps, localization and delineation. Localization addresses the question whether a shutter is present. Delineation determines the exact position and shape of the irradiation field. However, most approaches are restricted to certain assumptions, e.g. the collimation field must match a small set of form prototypes, have high-contrasted edges, is characterized by a certain grayscale, or, the algorithm is based on the simple hypothesis, that a collimation field is always present. In the latter case, only delineation is performed. Therefore, most existing methods are not applicable to large collections of radiographs from various modalities, such as obtained in the field of content-based image retrieval in medical applications (IRMA).⁸

In a recent approach, WIEMKER *et al.*¹⁶ have proposed the automated recognition of the collimation field in digital radiographs by maximization of the Laplace area integral. This versatile approach does *not* assume that the collimation field

- is a substantial fraction of the overall input image,
- is in a near-central position of the input image,
- is in parallel with the image boundary,
- is rectangular or matches a certain set of shape primitives, nor that it
- is build from a restricted number of edges.

In addition, the algorithm of WIEMKER *et al.* can cope with locally missing shutter edge contrast and low gradients. However, the approach is rather based on the hypothesis, that a shutter is present. In other words, collimation fields are frequently detected in radiographs that are routinely exposed, although they are not present. In order to reduce false positive detection, we present a simple extension to the algorithm and rigorously validate the resulting method on a large set of radiographs, which have been taken from daily routine.

2. METHOD OVERVIEW

The automatic collimation field detection is done in sequential steps. At first, all images are reduced in size to strengthen image gradients and reduce computing time. A fixed dimension is selected regardless of the initial size and aspect ratio to emphasize shorter edges in non-quadratic collimation fields or image formats. Local gradients are computed by means of directed Sobel templates and stored in the accumulator array of the Hough transform keeping the orientation of edges. Local maxima are detected within the accumulator array and used to generate hypotheses of shutter edges forming convex radiation fields. A greedy depth-first search strategy is applied to avoid exhaustive search within the hypotheses search space. Hypotheses are evaluated concerning four criteria:

1. maximize the density gradient perpendicular to the shutter gradient;
2. maximize the radiation density inside;
3. maximize the enclosed area;
4. minimize the variation of densities outside.

Parameterization A and B use criteria (1,2,3) and (1,2,3,4), respectively. Note that variant A corresponds to the initial approach of Wiemker *et al.*,¹⁶ while Criterion 4 is capable of reducing the number of positive collimator detection, which occurs frequently in skeleton radiographs from chest or skull if only the first three criteria are applied.

3. IMPLEMENTATION

3.1. Preprocessing and edge detection

Disregarding the aspect ratio, all images are resized to 128 x 128 pixels using linear interpolation.⁷ This preprocessing not only allows significant code optimization but also strengthens local gradients at the frame of the collimation field, makes small local gradient masks applicable and emphasizes the shorter lines of rectangular radiation fields.

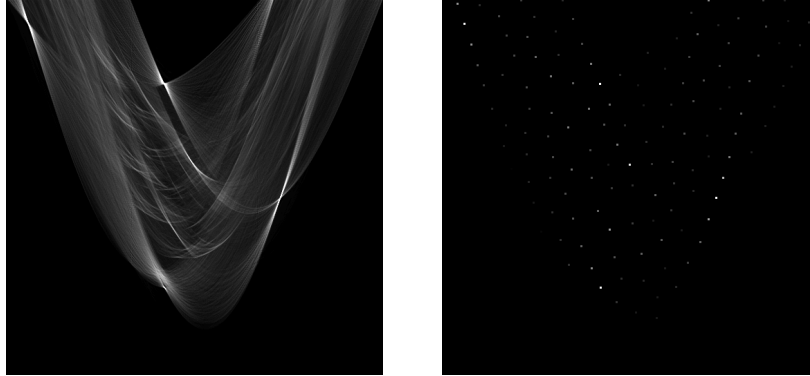


Fig. 1: Accumulator array of the Hough transform (left) and detection of local maxima (right).

In this work, the Sobel edge detection technique is applied yielding information about edge direction and magnitude. Next, a process is adopted from the Canny edge detection technique,² which is known as non-maximum suppression.¹² This step essentially locates the highest points in the edge magnitude data. It is performed by using edge direction information to check whether points are at the peak of a ridge. Given a region of 3×3 pixels, a point is at a maximum if the gradient at either side of it is less than the gradient at the center point.

3.2. Hough transform

The Hough transform⁵ is applied to detect straight lines in the resultant edge image. In contrast to this initial implementation, where the source image is considered to be a binary image, edge magnitudes are used to weight the votes cast by a pixel in the edge image. The result is a set of line parameters in foot-of-normal parameterization together with the number of votes cast for each line representation. In addition, the Hough transform has been extended by a third dimension. Every edge point is classified according to its edge direction to give evidence to the orientation of the line that it contributes to. The part of a line that corresponds to a shutter edge candidate consists of many edge points, which all have almost the same edge direction. As a line crosses the entire image plane, there may be edge points on the line that do not belong to this shutter edge but to another edge resulting from anatomical structure or noise. It is not desirable that those edge points contribute votes to the line that represents the shutter edge candidate in the accumulator array. It is likely that in most cases, the edge direction of those points is different from that of points, which belong to the shutter edge candidate.

All edge points belong to one of two classes: edge points that point to one and to the other side of the line. Actually, both classes take votes from edge points with edge direction from a range of 180° . On an ideal line, all edge points have an edge direction of $-\theta$ or $-\theta+180^\circ$ according to the orientation of the line. A line can represent a gradient from bright to dark and vice versa. Thus the two classes are

- edge points with an edge direction in the range $-\theta \pm 90^\circ$ and
- edge points with an edge direction in the range $-\theta + 180^\circ \pm 90^\circ$.

Therefore, when an edge point casts votes to a line in the accumulator array defined by its direction θ and its normal distance ρ to the origin, it only adds votes to the class it belongs to, according to the edge direction and θ . This ensures that edge points having opposite directions, which suggests that they do not belong to the same connected edge, consequently do not contribute to the same class of the third dimension of the accumulator array.

Finally, this three-dimensional array is transformed into a two-dimensional array with votes and orientation assigned to each entry of the two-dimensional plane. This is achieved by determining the maximal votes of the third dimension for every point on the two-dimensional plane of the three-dimensional accumulator array. Those votes are assigned to the new two-dimensional array. The orientation is determined by the class where the maximum was found. Accordingly, the orientation can be either $-\theta$ or $-\theta+180^\circ$. Note that the orientation of a line is defined in terms of edge direction. Thus, the orientation of a line represents the main edge direction of edge points on this line.

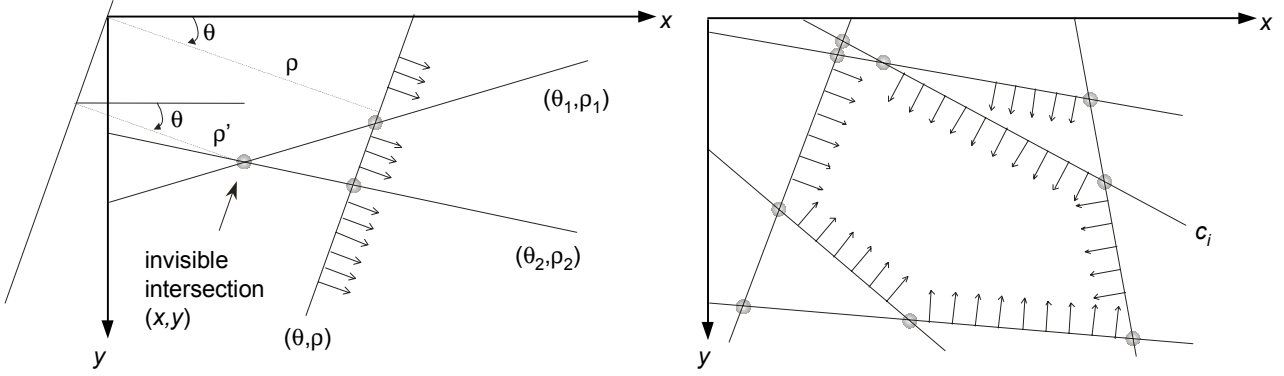


Fig. 2: Determination of invisible edges (left) and a set of shutter edges forming a hypothesis of the collimation field (right), where the hypothesis c_i has just been switched on.

3.3. Maximum detection

Now, the resultant accumulator array is analyzed in order to find local maxima concerning votes in the Hough domain, which correspond to actual edges in the resized original image. This is achieved by grouping points into regions in the accumulator array, which represent separated lines. Accordingly, all points belonging to the same region correspond to the same line. The parameters (θ, ρ) of the line corresponding to a region equal the parameters of the maximum of that particular region.

First, a list of all points in the accumulator array with their parameters (θ, ρ) , assigned votes, and orientation, is formed and sorted by votes with highest votes first. Thereafter, the list is explored from top to bottom. For each entry, it is checked whether it can be attached to an existing region, which is the case if its distance to the center of that particular region is smaller or equal to a certain region radius. For accumulator arrays of 180×180 cells, a radius of 10 cells has been chosen. If such a region is found, the point is attached to that region. Otherwise, a new region is created. A region is characterized by its center, which is the first point added to this region. This also is the region's maximum concerning the votes that are assigned to each point. The center and maximum does not change while new points are attached to the region. Accordingly, it is not necessary to keep track of the points that are added to a region. The total number of regions found can be influenced by adjusting the region radius. Figure 1 exemplifies an accumulator array and its corresponding local maxima.

3.4. Compiling hypotheses for collimation fields

The lines obtained in the previous step represent possible shutter edges. For accumulator arrays of 180×180 cells and a region radius of 10 cells, this list contains about 100 to 150 lines. The four image boundaries are added to this line list because image borders also are potential shutter edges. A collimation field hypothesis is a convex contour formed by several lines from the list of shutter edge candidates. A collimation field hypothesis is represented by a hypothesis vector

$$c = [c_1 \dots c_N]^T \quad (1)$$

where each edge candidate can either be part of the hypothesis or not, i.e., be switched on or off. An entry of the hypothesis vector c_i is 1 if and only if the i -th shutter edge candidate is switched on, and 0 otherwise.

Given a set of lines that form a hypothesis, those lines have several intersections with each other. The actual contour of the region defined by a hypothesis results from the line segments between intersections that are not occluded by any other shutter edge candidate (Fig. 2). Here, the orientation of a line is taken into account. Let us consider an image with the shuttered area being bright. In this case, every shutter edge has an orientation that points toward the center of the image. Accordingly, a shutter edge candidate shields everything that lies in the direction opposite to the edge direction.

The set of line segments that are not occluded by any other shutter edge candidate is found by eliminating all invisible intersections, i.e., intersections that are covered by another shutter edge candidate. An intersection (x, y) of two lines (θ_1, ρ_1) and (θ_2, ρ_2) is obtained from

$$x = \frac{\rho_2 \sin \theta_1 - \rho_1 \sin \theta_2}{\cos \theta_2 \sin \theta_1 - \cos \theta_1 \sin \theta_2} \quad (2)$$

$$y = \frac{\rho_2 \cos \theta_1 - \rho_1 \cos \theta_2}{\sin \theta_2 \cos \theta_1 - \sin \theta_1 \cos \theta_2} \quad (3)$$

To determine whether an intersection is hidden by a particular shutter edge candidate (θ, ρ) , the distance ρ' concerning the angle θ is calculated for the intersection (x, y) (Fig. 2). If ρ' is smaller than ρ of that specific shutter edge candidate, this intersection is invisible. For dark shutter areas or line orientations pointing from right to left, e.g., at right edges of a collimation field hypothesis with a bright shuttered area, invisible intersections are determined analogously. This process is executed for every pair of a shutter edge candidate and an intersection while effectively removing all invisible intersections. Line segments between remaining visible intersections form the contour of the collimation field hypothesis.

3.5. Evaluation of collimation field hypotheses using the Laplace area integral

Each hypothesis that was formed following the procedure described above, is evaluated by means of an objective function assessing four attributes of the hypothesis, i.e., the contour that is formed from the set of lines that represent the hypothesis:

1. the sum of the gradient over the contour;
2. the radiation density of the enclosed area;
3. the area that is enclosed by the contour;
4. the number of different gray-levels outside the contour.

The aim is to maximize the gradient over the contour, enclosed radiation density, and the enclosed area while minimizing the number of different gray-levels outside the contour.

The enclosed area is simply the number of pixels inside the contour. The radiation density of the enclosed area is the sum of the radiation at each pixel within the contour divided by the enclosed area. The radiation at a pixel depends on the brightness level at that particular pixel and the brightness of the shuttered area. If the shuttered area, i.e., the area where little radiation had passed through the object, is bright, gray-levels are logarithmically proportional to the radiation attenuation. If the area outside the contour is dark, gray-levels are in inverse proportion to radiation attenuation. The sum of the gradient over the contour can be calculated by the sum of the Laplace values within the contour.¹⁶ This is known as the divergence theorem, which expresses the equivalence of a contour integral over a vector field and an area integral over the divergence of the vector field. Note that in a discrete domain, this theorem does not exactly hold true. However, the sum of the Laplace values within the contour is a reasonable approximation of the actual sum of the gradient over the contour. The number of different gray-levels outside the contour is evaluated by an analysis of the histogram of the shuttered area.

To speed up calculations, cumulative images of the original gray-level image and the image with Laplace values are calculated. Successively, a sum of pixels within the contour can be computed by subtracting pixels in the cumulative images that lie on left edges and adding pixels in the cumulative images that lie on right edges of the contour. The task of finding pixels that lie on left and right edges of the contour is not trivial. In this work, this is achieved by an adapted polygon filling algorithm. The original polygon filling algorithm³ draws pixels on spans between left and right edges of a polygon. In this work, only the border pixels that lie strictly within the polygon, i.e., the contour, are considered and used as described above. Those border pixels are also used to calculate the enclosed area and to determine the area outside the contour, from which the histogram is evaluated.

3.6. Optimization by greedy depth-first search strategy

An exhaustive search of the hypothesis space of order $O(2^N)$ built from $N \approx 100$ shutter edge candidates cannot be conducted. Instead, a greedy depth-first search strategy is applied. WIEMKER *et al.*¹⁵ have tested this approach for sufficiency by performing exhaustive searches of the hypothesis space for lower numbers N . The first hypothesis is the null hypothesis, i.e., only the image boundaries are turned on as shutter edge candidates. Then, all N shutter edge candidates are tentatively switched on, one at each time. The objective function is evaluated for every trial and the edge candidate yielding the highest result of the objective function is switched on permanently. This is continued in the next recursion, where again all of the $N - 1$ remaining in-active edge candidates are tentatively switched on in addition to the first. Again, the candidate with the highest yield is then switched on permanently. This procedure is continued until none of the trials yields any increase in the objective function value.

After this single-track depth search, which does not fully explore any branches of the search tree, a restricted width search is conducted to check the consistency of the initial optimum hypothesis c . Let the preliminary optimum have K of the N shutter edge candidates switched on. Then, a greedy depth-first search is performed again with each of these K candidates switched on as the first shutter edge after the null hypothesis. If one of the K depth-first searches returns with a different edge set c' with K' edges turned on and an objective function value which is larger than the preliminary optimum, then this solution is adopted as the new preliminary optimum and the search starts again for all K' edges as starting points. Only if none of the K' depth-first searches returns with an objective function value higher than the preliminary optimum, the search terminates and the optimal edge set is fixed. Although the number of searching steps is not guaranteed to be small, in practice only a few searches need to be performed before termination of the algorithm.

This search is conducted twice. First, the shuttered area is considered to be dark. After that, the collimation field is looked at as being bright. Then, the maximum of the two runs is selected as the optimal edge set together with the information about the shuttered area's density.

3.7. Visualization

From this optimal edge set, the line segments between visible intersections of the shutter edges are determined. This contour is extrapolated to the initial size of the original input image, which has not been resized. This extrapolated contour is used to define a mask segment for the original image where points within and outside the contour are defined as valid and invalid, respectively. This mask is applied to further evaluation. In addition, the line segments can be used to draw the collimation field in the resized image for visualization purposes. Figure 3 shows successful delineation for rectangular, circular, and polygonal radiation fields.

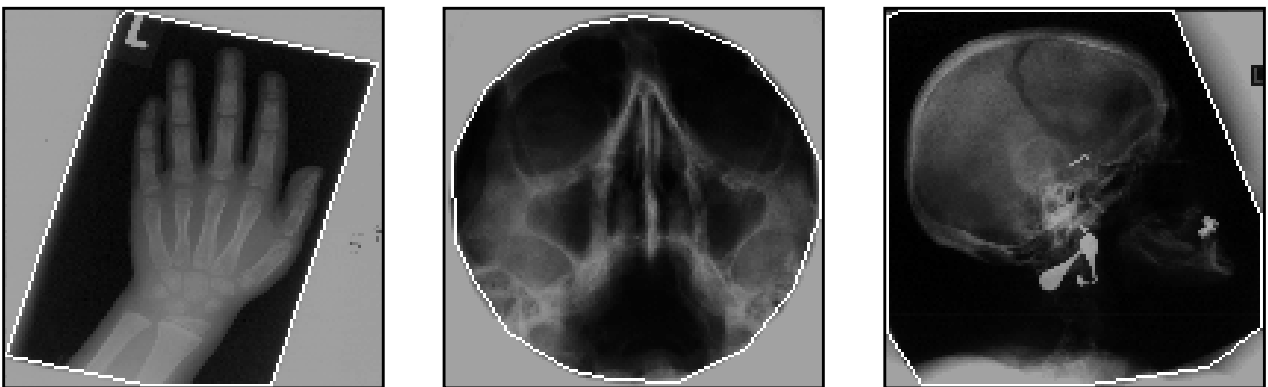


Fig. 3: Visualization of a rectangular (left), circular (middle), and polygonal (right) radiation field.

image subset	set of parameters	training			evaluation		
		sensitivity	specificity	precision	sensitivity	specificity	precision
0	A	0.46	0.97	0.87	0.46	0.96	0.87
	B	0.62	0.99	0.91	0.52	0.98	0.89
1	A	0.33	0.97	0.85	0.36	0.98	0.86
	B	0.47	0.98	0.89	0.56	0.99	0.90
2	A	0.53	0.97	0.88	0.52	0.95	0.87
	B	0.48	0.98	0.89	0.56	0.99	0.90
3	A	0.53	0.97	0.88	0.45	0.96	0.87
	B	0.74	0.98	0.93	0.61	0.97	0.90
4	A	0.48	0.97	0.87	0.46	0.96	0.87
	B	0.58	0.98	0.90	0.55	0.99	0.90
5	A	0.29	0.97	0.82	0.37	0.98	0.87
	B	0.49	0.99	0.88	0.56	0.98	0.90
6	A	0.56	0.97	0.90	0.45	0.96	0.86
	B	0.63	0.99	0.93	0.54	0.99	0.90
7	A	0.51	0.97	0.90	0.46	0.96	0.86
	B	0.55	0.98	0.91	0.55	0.99	0.90

Tab. 1: Results of cross-validation. The marked boxes are referred to from the body text.

4. EVALUATION

In total, 4,000 radiographs (763 with shutter edges) were randomly selected from clinical routine at the University Hospital, Aachen, Germany, including any modality of projective X-ray examinations. Note that a number of 4,000 references has been used by FDA (United States Food and Drug Administration) to validate software algorithms that screen normal head CT studies from studies that contain pathology.¹ Eight subsets (each of 500 images) were obtained randomly. A set of 500 images was used to optimize the parameters, i.e. the weights combining the criteria mentioned above. With respect to its application in content-based image retrieval, false positive location is to be avoided. Therefore during the manual parameterization, the specificity was tuned to be as large as 97% and 98% for parameter sets A and B, respectively. Note that a higher specificity was not possible for all eight sets of 500 training images. Using this sets of parameters, the evaluation was based on the corresponding 3,500 images. This process was repeated for all eight possible combinations of a 500 image subset and remaining 3,500 images.

5. RESULTS

For quantitative evaluation, only collimator segments covering more than 5% of the image area were considered as such. In case of any shutter segment, which has not been detected (false location) or any shutter segment, which has been detected although not present (false delineation), an error was recorded (Fig. 4). Table 1 summarizes the results. During the training phase, the sensitivity of variant B was up to 21 percentage points higher than that of variant A (see subset no. 3) although the specificity also was one or two points higher. Hence, the precision of variant A is always below that of variant B. Only for one case (see subset no. 2), variant A was superior to variant B with respect to the sensitivity. In general, these results were confirmed by the 3,500 reference images, which had not been seen during the training phase. Here, variant B was superior to variant A in all cases with respect to both sensitivity and precision. Nonetheless, if a high specificity of collimation field detection is enforced, the sensitivity is below 60% in almost all cases. The resulting overall precision is 86,6% and 89,9% for variant A and B, respectively.

6. DISCUSSION

Automatic delineation of collimation field is rather simple when the presence of shutter edges can be assumed, e.g. the algorithm is applied to a certain digital modality. With our approach, collimation fields are reliably detectable in any radiograph. The specificity of our algorithm is up to 99%. This figure is obtained from a rigorous evaluation that is based on 4,000 radiographs, which has not yet been reported for any method of collimation field detection.

Although only a very small number of parameters needs adjustment, i.e., the three relative weights combining the four criteria, and manual parameterization is performed using a very large number of 500 arbitrarily chosen images, the overall precision of training and evaluation decreases in two of the eight cases (25%) about as much as three percentage points (see subsets no. 3 and no. 6). Concerning the sensitivity of variant B, figures range about 9 percentage points from as low as 52% (see subset no. 1) up to 61% (see subset no. 3). In other words, the number of used images is still too small to allow absolute generalization of the results.⁹ However, validation of algorithms for medical image processing is often based on a significant smaller number of images.

The proposed algorithm does not assume a certain set of form archetypes and detects shutters from any number of edges including curved shapes. Incorporating a Hough transform, the algorithm can cope with local missing shutter information. Overcoming a basic restriction of previous approaches, automatic collimation field detection now becomes available for a large range of applications such as content-based image retrieval in medical applications.

ACKNOWLEDGEMENT

This work was partly supported by the German Research Community (Deutsche Forschungsgemeinschaft, DFG) grant Le 1108/4-1.

REFERENCES

1. C. W. Brown, "Building a Medical Image Processing Algorithm Verification Database," *Proceedings SPIE Medical Imaging*, **3979**, pp. 772–780, 2000.
2. J. Canny, "A Computational Approach to Edge Detection," *IEEE Transactions on Pattern Analysis and Machine Intelligence* **8**, pp. 679–698, 1986.
3. S. N. C. Cheng, H.-P. Chan, L. T. Niklason, and R. S. Adler, "Automated Segmentation of Regions of Interest on Hand Radiographs," *Medical Physics* **21(8)**, pp. 1293–1300, 1994.
4. P. Dewaele, M. Ibison, and P. Vuylsteke, "A Trainable Rule-Based Network for Irradiation Field Recognition in AGFA's ADC System," *Proceedings SPIE Medical Imaging* **2708**, pp. 72–84, 1996.
5. R. O. Duda and P. E. Hart, "Use of the Hough Transformation to Detect Lines and Curves in Pictures,"

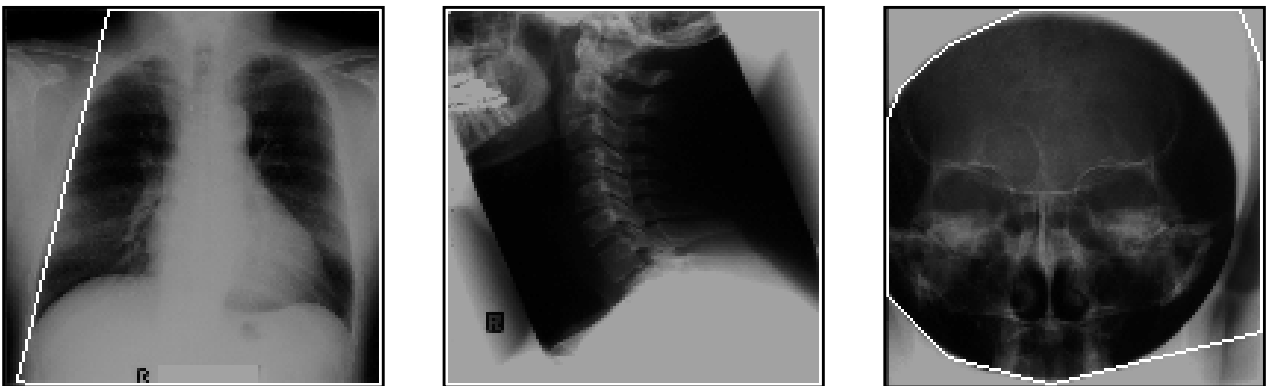


Fig. 4: False location (left) and false delineation (middle and right).

Communications of the ACM **15**, pp. 11–15, 1972.

6. J. D. Foley, J. F. Hughes, S. K. Feiner, and R. L. Phillips, *Computer Graphics: Principles and Practice*, Addison Wesley, second edition, 1995.
7. T. M. Lehmann, C. Gönner, and K. Spitzer: Survey: Interpolation Methods in Medical Image Processing. *IEEE Transactions on Medical Imaging* **18(11)**, pp. 1049–1075, 1999.
8. T. M. Lehmann, B. Wein, J. Dahmen, J. Bredno, F. Vogelsang, and M. Kohnen, "Content-Based Image Retrieval in Medical Applications: A Novel Multi-Step Approach," *Proceedings SPIE Medical Imaging* **3972**, pp. 312–320, 2000.
9. T. M. Lehmann, "From Plastic to Gold: A Unified Classification Scheme for Reference Standards in Medical Image Processing," *Proceedings SPIE Medical Imaging*, contents of this volume, 2002.
10. J. Lou and R. A. Senn, "Collimation Detection for Digital Radiography," *Proceedings SPIE Medical Imaging* **3034**, pp. 74–85, 1997.
11. Y. Lu and H. Guo, "Background Removal in Image Indexing and Retrieval," *Proceedings 10th Int. Conf. Image Analysis and Processing, IEEE Computer Society*, pp. 933–938, 1999.
12. M. Sonka, V. Hlavac, and R. Boyle, "Image Processing, Analysis, and Machine Vision," 2nd edition, Brooks/Cole Publishing Company, 1999.
13. H. Wang and B. G. Fallone, "A Robust Morphological Algorithm for Automatic Radiation Field Extraction and Correlation of Portal Images," *Medical Physics* **21(2)**, pp. 237–244, 1994.
14. H. Wang and B. G. Fallone, "A Mathematical Model of Radiation Field Edge Localization," *Medical Physics* **22(7)**, pp. 1107–1110, 1995.
15. R. Wiemker, S. Dippel, M. Stahl, and T. M. Buzug, "A Graph-Based Approach to Automated Shutter Detection in Digital X-ray Images," *Proceedings CARS'99 Computer Assisted Radiology and Surgery*, pp. 14–18, 1999.
16. R. Wiemker, S. Dippel, M. Stahl, T. Blaffert, and U. Mahlmeister, "Automated Recognition of the Collimation Field in Digital Radiography Images by Maximization of the Laplace Area Integral," *Proceedings SPIE Medical Imaging* **3979**, pp. 1555–1565, 2000.
17. J. Zhang and H. K. Huang, "Automatic Background Recognition and Removal (ABRR) in Computed Radiography Images," *IEEE Transactions on Medical Imaging* **16(6)**, pp. 762–771, 1997.